

Ptpn11 deletion in a novel progenitor causes metachondromatosis by inducing hedgehog signalling

Wentian Yang¹, Jianguo Wang¹, Douglas C. Moore¹, Haipei Liang¹, Mark Dooner², Qian Wu³, Richard Terek¹, Qian Chen¹, Michael G. Ehrlich¹, Peter J. Quesenberry² & Benjamin G. Neel⁴

The tyrosine phosphatase SHP2, encoded by *PTPN11*, is required for the survival, proliferation and differentiation of various cell types^{1,2}. Germline activating mutations in *PTPN11* cause Noonan syndrome, whereas somatic *PTPN11* mutations cause childhood myeloproliferative disease and contribute to some solid tumours. Recently, heterozygous inactivating mutations in *PTPN11* were found in metachondromatosis, a rare inherited disorder featuring multiple exostoses, enchondromas, joint destruction and bony deformities^{3,4}. The detailed pathogenesis of this disorder has remained unclear. Here we use a conditional knockout (floxed) *Ptpn11* allele (*Ptpn11^{fl/fl}*) and Cre recombinase transgenic mice to delete *Ptpn11* specifically in monocytes, macrophages and osteoclasts (lysozyme M-Cre; *LysMCre*) or in cathepsin K (Ctsk)-expressing cells, previously thought to be osteoclasts. *LysMCre;Ptpn11^{fl/fl}* mice had mild osteopetrosis. Notably, however, *CtskCre;Ptpn11^{fl/fl}* mice developed features very similar to metachondromatosis. Lineage tracing revealed a novel population of CtskCre-expressing cells in the perichondrial groove of Ranvier that display markers and functional properties consistent with mesenchymal progenitors. Chondroid neoplasms arise from these cells and show decreased extracellular signal-regulated kinase (ERK) pathway activation, increased Indian hedgehog (*Ihh*) and parathyroid hormone-related protein (*Pthrp*, also known as *Pthlh*) expression and excessive proliferation. Shp2-deficient chondroprogenitors had decreased fibroblast growth factor-evoked

ERK activation and enhanced *Ihh* and *Pthrp* expression, whereas fibroblast growth factor receptor (FGFR) or mitogen-activated protein kinase (MEK) inhibitor treatment of chondroid cells increased *Ihh* and *Pthrp* expression. Importantly, smoothed inhibitor treatment ameliorated metachondromatosis features in *CtskCre;Ptpn11^{fl/fl}* mice. Thus, in contrast to its pro-oncogenic role in haematopoietic and epithelial cells, *Ptpn11* is a tumour suppressor in cartilage, acting through a FGFR/MEK/ERK-dependent pathway in a novel progenitor cell population to prevent excessive *Ihh* production.

Cartilage tumours, including exostoses, enchondromas and chondrosarcomas, comprise ~20% of skeletal neoplasms⁵. Benign and malignant cartilaginous tumours can arise sporadically, but cartilage tumour syndromes, including hereditary multiple exostoses, the multiple enchondromatosis disorders (Ollier disease and Maffucci syndrome) and metachondromatosis, also exist^{6,7}. The cellular and molecular pathogenesis of most cartilage tumours is incompletely understood.

Metachondromatosis is an autosomal dominant tumour syndrome featuring multiple exostoses and enchondromas^{6,7}. Recently, heterozygous early frameshift or nonsense mutations in *PTPN11* were identified in >50% of metachondromatosis cases^{3,4}. *PTPN11* encodes the non-receptor protein tyrosine phosphatase SHP2, which is required for RAS/ERK pathway activation in most receptor tyrosine kinase, cytokine receptor, and integrin signalling pathways^{1,2}. Germline activating

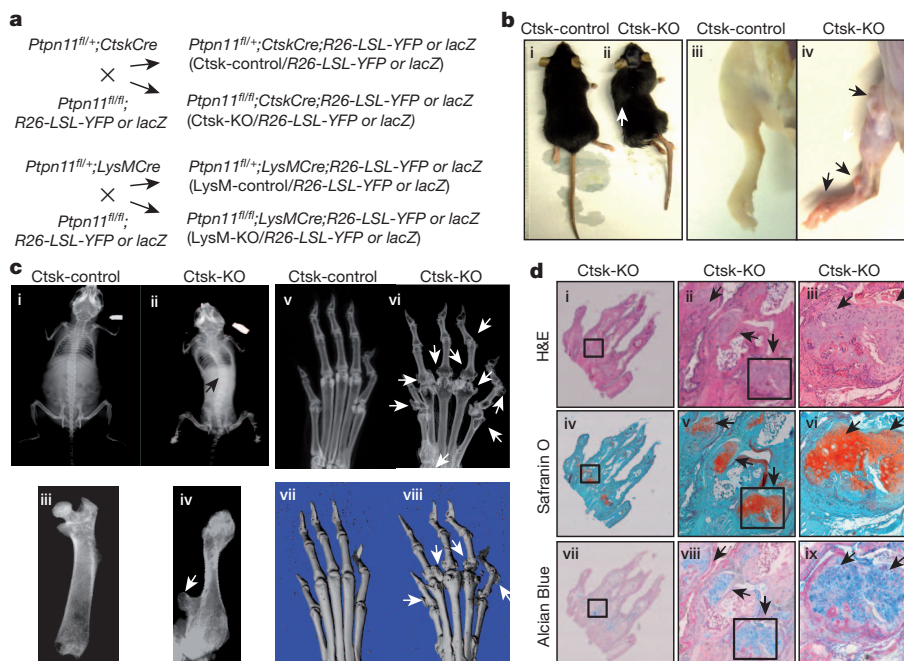


Figure 1 | *Ptpn11* deletion in Ctsk-expressing cells causes metachondromatosis. **a**, Schemes for generating Ctsk-KO, LysM-KO and control mice. **b**, **c**, Gross images (**b**) and Faxitron/μ-CT radiographs (**c**) of 12-week-old Ctsk-KO mice showing dwarfism and scoliosis (**b** ii, white arrow; **c** ii, black arrow), increased bone mineral density (**c** ii, iv; arrows) and multiple exostoses of knees, ankles and metatarsals (**b** iv and **c** ii, iv, vi, viii; arrows) with joint destruction. **d**, Sagittal sections of metatarsal joints stained with haematoxylin and eosin (H&E; i–iii), Safranin O (iv–vi) and Alcian Blue (vii–ix) showing cartilaginous exostoses and enchondromas (arrows) in Ctsk-KO mice. Images in i, iv, vii are magnified ×2, in ii, v, viii ×10 and in iii, vi, ix ×20. Images in ii, v, viii and iii, vi, ix are magnified (×10) views of boxed areas in i, iv, vii and ii, v, viii, respectively. Data shown are representative images; each analysis was performed on at least five mice per genotype.

¹Department of Orthopaedics, Brown University Alpert Medical School and Rhode Island Hospital, Providence, Rhode Island 02903, USA. ²Department of Medicine and COBRE Center for Stem Cell Biology, Rhode Island Hospital and Brown University Alpert Medical School, Providence, Rhode Island 02903, USA. ³Department of Pathology and Laboratory Medicine, University of Connecticut Health Center, Farmington, Connecticut 06030, USA. ⁴Princess Margaret Cancer Center, University Health Network, and Department of Medical Biophysics, University of Toronto, Toronto, Ontario M5G 1L7, Canada.

mutations in *PTPN11* cause Noonan syndrome, whereas mutations that impair SHP2 catalytic activity cause LEOPARD syndrome (an acronym for multiple lentigenes, ECG conduction abnormalities, ocular hypertelorism, pulmonic stenosis, abnormal genitalia, retardation of growth and sensorineural deafness), both of which can feature skeletal abnormalities⁸. Somatic activating mutations in *PTPN11* are the most common cause of juvenile myelomonocytic leukaemia and contribute to other leukaemias and some solid tumours^{1,2}. Although *PTPN11* is a well-established human oncogene, it is unclear how heterozygous loss-of-function *PTPN11* alleles cause cartilage neoplasms.

Global *Ptpn11* deletion results in early embryonic lethality^{9,10}, whereas postnatal deletion has context-dependent effects^{1,2}. To assess the role of Shp2 in osteoclasts, we crossed *Ptpn11*^{fl/fl} mice¹⁰ to mice expressing Cre under the control of the endogenous *LysM*¹¹ or *Ctsk*¹² promoter. The *LysM* promoter is active in monocytes, macrophages and osteoclast precursors¹¹, whereas the *Ctsk* promoter reportedly is active only in mature osteoclasts^{12,13}. These crosses generated *Ptpn11*^{fl/+};*LysMCre* and *Ptpn11*^{fl/fl};*LysMCre* (hereafter, *LysM*-control and *LysM*-knockout (KO)) and *Ptpn11*^{fl/+};*CtskCre* and *Ptpn11*^{fl/fl};*CtskCre* (hereafter, *Ctsk*-control and *Ctsk*-KO) mice, respectively (Fig. 1a).

Neither *LysM*-control nor *Ctsk*-control mice had a discernible phenotype, so we focused all subsequent analyses on *LysM*-KO and *Ctsk*-KO mice. Shp2 levels were reduced by >80% in bone-marrow-derived macrophages and osteoclasts in *LysM*-KO and *Ctsk*-KO mice (Supplementary Fig. 1a and data not shown). *LysM*-KO and *Ctsk*-KO mice were born at the expected Mendelian ratios and appeared to be normal for the first 3 weeks after birth. Subsequently, *LysM*-KO mice developed mild, age-related osteopetrosis (Supplementary Fig. 1b and data not shown). By contrast, within 8 weeks after birth, *Ctsk*-KO mice exhibited a dramatic skeletal phenotype, comprising decreased body length, increased bone mineral density, scoliosis, metaphyseal exostoses and markedly decreased mobility (Fig. 1b–d and Supplementary Video 1).

Sections of hindlimb paw and knee joints from 12-week-old *Ctsk*-KO mice revealed multiple exostoses and enchondromas at the metaphyses of their metatarsals and phalanges (Fig. 1d), tibiae and femurs (Supplementary Fig. 1c, d), and other bones (data not shown), features reminiscent of metachondromatosis. As heterozygous *PTPN11* frameshift mutations cause metachondromatosis^{3,4}, these findings indicate that *PTPN11* is a cartilage tumour-suppressor gene, and suggest that loss (or silencing) of the remaining *PTPN11* allele is required for tumour formation.

To identify the cells responsible for metachondromatosis-like disease in *Ctsk*-KO mice, we first injected bone marrow from 6-week-old *Ctsk*-KO and *Ctsk*-control mice (C57/BL6; CD45.2) into lethally irradiated 3-week-old recipients (B6.SJL; CD45.1). Recipient mice exhibited high chimaerism (Supplementary Fig. 2a, b), but did not develop cartilage tumours in over 12 months of observation. Consistent with the osteopetrosis seen in *LysM*-KO mice, recipients had increased bone mineral density (Supplementary Fig. 2c). Clearly, however, cartilage tumours in *Ctsk*-KO mice are not due to altered osteoclast development or function.

Next, we performed lineage-tracing studies using *Rosa26-lox-stop-lox-lacZ* (*R26-LSL-lacZ*) or *Rosa26-LSL-YFP* (*R26-LSL-YFP*) Cre reporter mice. Notably, *CtskCre*, but not *LysMCre*, was expressed in a subset of perichondrial cells within the so-called groove of Ranvier (Fig. 2a). Sections from knee joints collected at postnatal day (P)10 revealed expansion of a cluster of Alcian Blue/Safranin O-positive cells in this region in *Ctsk*-KO mice, but not in controls (Fig. 2b, boxed region and Supplementary Fig. 1c). By postnatal week 2, the yellow fluorescent protein (YFP)⁺ cell population had increased and differentiated into ectopic cartilaginous tissue in compound *Ctsk*-KO;YFP reporter mice (Fig. 2c, boxed region). Exostoses were palpable at 6 weeks and visible by 8–12 weeks. In compound *Ctsk*-KO;YFP reporter mice, these lesions consisted of YFP⁺ chondroid cells at various stages of development, including proliferating, pre-hypertrophic and hypertrophic

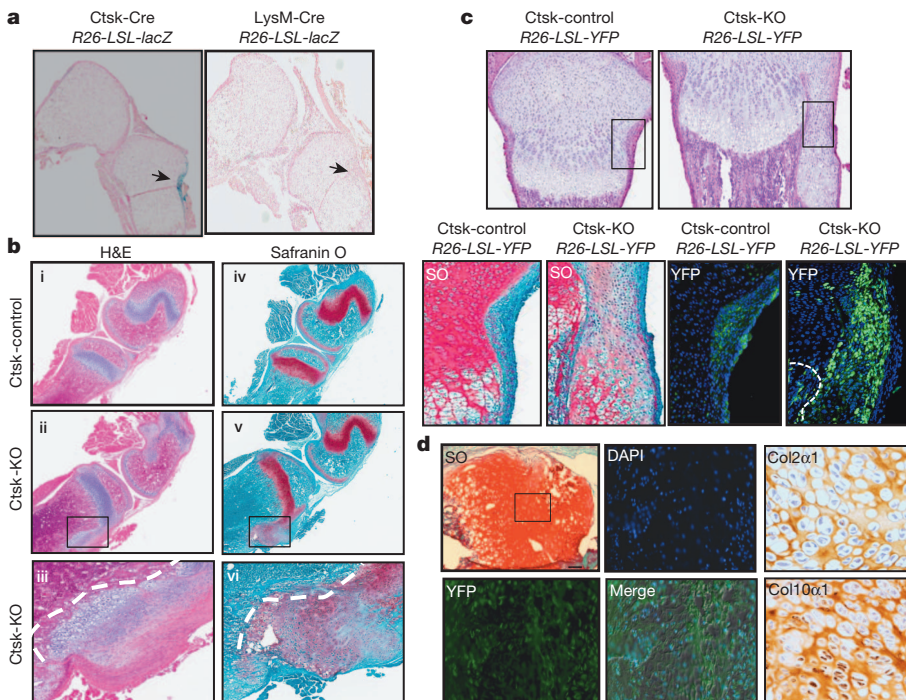


Figure 2 | Skeletal tumours in *Ctsk*-KO mice originate from perichondrial groove of Ranvier cells. **a**, 5-bromo-4-chloro-3-indolyl- β -D-galactoside (X-gal) staining of knee joint sections from 1-week-old *R26-LSL-lacZ*;*CtskCre* and *R26-LSL-lacZ*;*LysMCre* reporter mice showing that the *Ctsk* (but not the *LysM*) promoter is active not only in osteoclasts, but also in a subset of cells from the perichondrial groove of Ranvier (arrows). Images are magnified $\times 4$. **b**, Haematoxylin and eosin and Safranin O staining of knee joint sections from P10 *Ctsk*-control (i, iv) and *Ctsk*-KO (ii, iii, v, vi) mice showing expansion of cells within the perichondrial groove of Ranvier region in *Ctsk*-KO mice. Images i, ii, iv, v are magnified $\times 4$. Images in iii and vi are magnified ($\times 10$) views of boxed areas in ii and v, respectively. **c**, Haematoxylin and eosin and Safranin O (SO)-stained sections (magnified $\times 2$) showing expanding YFP⁺ population within the perichondrial groove of Ranvier (boxed region in top panels, magnified $\times 10$ below) that also stains with Safranin O, indicative of cartilage. Dashed line marks boundary between marrow/growth plate and perichondrial groove. **d**, Frozen section of an exostosis from the metatarsal joint of *Ctsk*-KO;YFP mice showing co-localization of YFP reporter with cartilaginous tumour cells (boxed area). SO panel, $\times 4$ magnification; all other panels, $\times 10$ magnification. Note that the lesion is enriched in proliferating and pre-hypertrophic chondrocytes, as shown by overlapping Col2 α 1 and Col10 α 1 immunostaining. Each panel is a representative image from one mouse; each analysis was performed on at least three mice per genotype. DAPI, 4',6-diamidino-2-phenylindole.

chondrocytes, as revealed by cell morphology and *Col2a1* and *Col10a1* immunostaining (Fig. 2c, d and data not shown). Notably, nearly all chondroid tumour cells were YFP⁺ (Fig. 2c and Supplementary Fig. 2d). Hence, cartilaginous tumours in Ctsk-KO mice (and, by analogy, most likely in metachondromatosis) result from cell-autonomous lack of Shp2 in Ctsk⁺ cells from the perichondrial groove of Ranvier.

The perichondrial groove of Ranvier is believed to contain chondroprogenitors responsible for circumferential cartilage growth, but these cells are not well-characterized^{14,15}. We used flow cytometry to analyse epiphyseal cartilage cells collected from the distal femurs and proximal tibiae of Ctsk-control;YFP and Ctsk-KO;YFP mice at P10–12. Compared with controls, the frequency of YFP⁺ cartilage cells in Ctsk-KO;YFP mice was increased by ~fivefold (Fig. 3a). Within the YFP⁺ cell population, the percentage of cells expressing CD44, CD90 and CD166 (mesenchymal progenitor markers), but not CD31 (endothelial cell marker), also was increased (Fig. 3b). Staining for the stromal cell antigen Stro-1 in addition to jagged 1, markers associated with presumptive chondroprogenitors in the groove on the basis of BrdU label retention studies¹⁶, was more intense in Ctsk-KO mice (Fig. 3c). Moreover, YFP⁺ cells were capable of multi-lineage differentiation *in vitro*, as assessed by Alcian Blue, Oil Red O and Alizarin Red staining, respectively (Fig. 3d). These data indicate that Shp2 regulates the proliferation of a novel cartilage cell population characterized by Ctsk expression, which we hereafter term Ctsk⁺ chondroid progenitors (CCPs).

Multiple pathways control cartilage development and homeostasis¹⁷. IHH and PTHRP signalling are particularly important, and aberrant regulation of these pathways causes developmental defects and skeletal tumours^{18,19}. We examined chondrogenic gene expression in cartilage tumours from Ctsk-KO mice by quantitative reverse-transcription PCR (qRT-PCR). Consistent with our immunostaining data (Fig. 2d), *Col2a1* and *Col10a1* transcripts were increased. Furthermore, *Ihh* and *Pthrp* levels were increased substantially (Fig. 4a and Supplementary Fig. 3a).

These findings prompted us to ask whether Shp2 regulates *Ihh* and *Pthrp* production, and if so, how. During development, cells within the perichondrium make Fgf18, which can signal to adjacent cells via Fgfr3 to suppress *Ihh* expression^{20,21}. As Shp2 is required for Fgfr signalling in other cell types^{1,2}, we suspected that Shp2 might be required for Fgfr3-induced suppression of *Ihh* expression. We therefore examined the status of Fgfr3 signalling components and *Ihh* expression in CCPs. Erk activation, as assayed by Tyr 204 Thr 202 phosphorylation, was compromised in the absence of Shp2, whereas Akt (phospho (p)-Ser 473) and Stat1/3 (p-Tyr 807) activation were unaffected (Fig. 4a, Supplementary Fig. 3b and data not shown). Furthermore, consistent with our qRT-PCR data, *Ihh* messenger RNA and protein were increased in Shp2-deficient CCPs (Fig. 4a). *Ihh* antibody specificity was confirmed by immunostaining of growth plate cartilage (Supplementary Fig. 3c).

CCPs are rare, rendering their detailed biochemical analysis unfeasible. We therefore tested the effects of Shp2 depletion in ATDC5 chondroid cells by stably expressing either of two short hairpin RNAs (shRNAs) targeting mouse *Ptpn11*. As in Ctsk-KO mice (Fig. 4a), Fgf18-evoked Erk activation was decreased, whereas *Ihh* and *Pthrp* levels were increased in Shp2-deficient cells (Fig. 4b). Conversely, FGFR (PD173074) or MEK (UO126) inhibition led to enhanced *Ihh* and *Pthrp* expression in parental ATDC5 cells (Fig. 4c).

Ihh signalling evokes *Pthrp* production²². Our data, in addition to previous studies²³, suggested that increased *Ihh* levels might be pathogenic in metachondromatosis. If so, then blocking or attenuating *Ihh* signalling might slow and/or prevent the disease. To test this hypothesis, control (wild-type) and Ctsk-KO mice (9 per group) were gavaged daily with the smoothed inhibitor PF-04449913 (SMOi, 100 µg g⁻¹ body weight) or vehicle control (0.5% methylcellulose), beginning at 5 weeks of age (when early lesions were present) and continuing for the succeeding 4 weeks. Skeletal phenotype was assessed by X-ray, micro-computed tomography (µ-CT) and histology. Notably, SMOi treatment significantly reduced the number of exostoses in Ctsk-KO

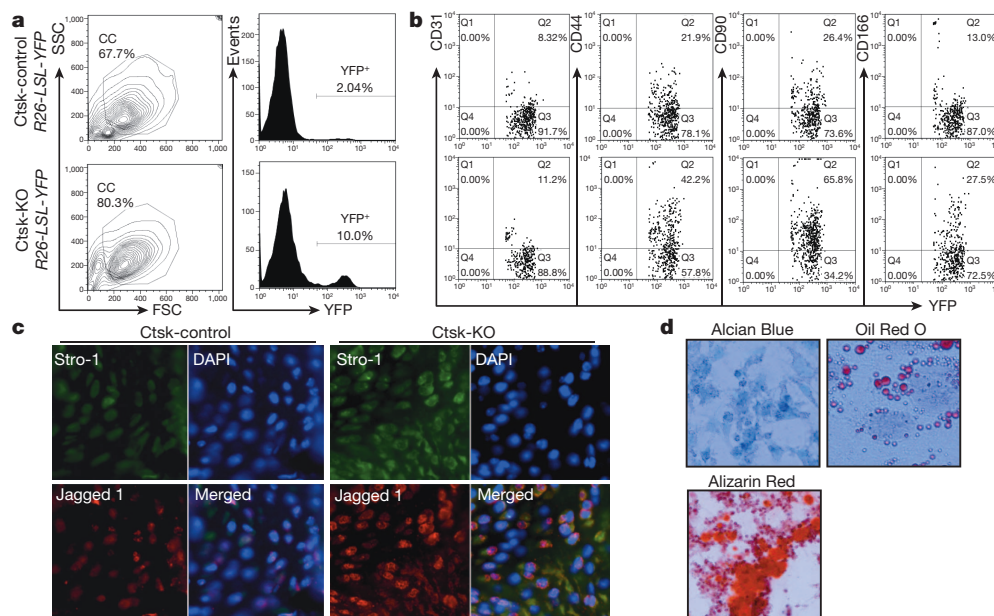


Figure 3 | *Ptpn11* deletion in Ctsk-expressing cells causes expansion of novel chondroprogenitor cell population within the perichondrial groove of Ranvier. **a**, Flow cytometric analysis showing YFP⁺ cells from pooled epiphyseal cartilage from 5–7 Ctsk-control;YFP mice; note increased percentage of such cells in 2-week-old Ctsk-KO;YFP mice. CC, chondroid cells. **b**, Flow cytometric analysis of YFP⁺ perichondrial cells showing staining for CD31, CD44, CD90 and CD166. Data in panels **a** and **b** are from a single experiment; similar results were obtained in two additional experiments. **c**, Immunofluorescence micrograph (magnified $\times 20$) showing Stro-1 and

jagged 1 expression in YFP⁺ perichondrial cells. Nuclei are stained with DAPI. Note enhanced intensity of Stro-1 and jagged 1 staining in Ctsk-KO cells. Data shown are from single mice of each genotype; two additional mice were analysed for each genotype with similar results. **d**, CCPs give rise to cartilage, fat and bone. Fluorescent-activated cell sorting (FACS)-purified YFP⁺ cells from 5–7 mice were subjected to differentiation assays in triplicate. After 2–3 weeks of culture (see Methods), cells were fixed and stained with Alcian Blue, Oil Red O and Alizarin Red to visualize the formation of cartilage, fat and bone tissue (magnified $\times 20$), respectively.

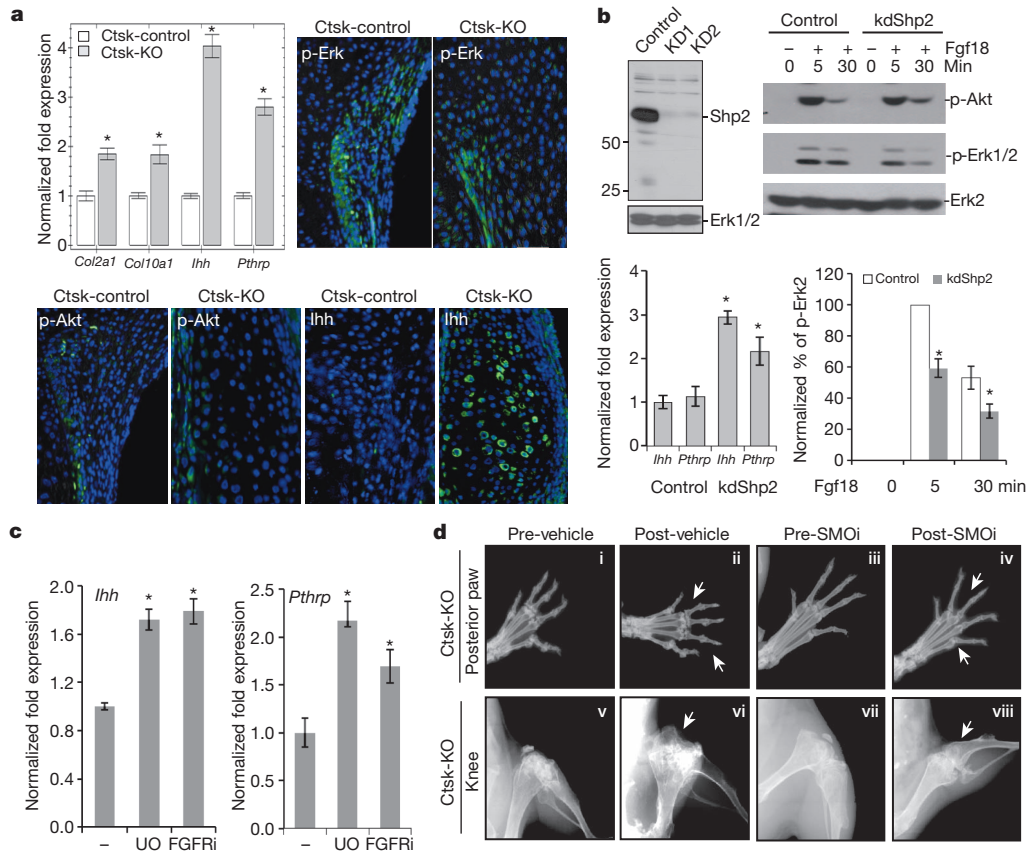


Figure 4 | Shp2 deficiency impairs Erk activation but promotes *Ihh* and *Pthrp* expression. **a**, Top left, qRT-PCR showing increased *Col2a1*, *Col10a1*, *Ihh* and *Pthrp* expression in laser-captured cartilaginous cells from exostoses in four mice per genotype, compared with normal articular cartilage cells (mean \pm s.d.; * $P < 0.05$, two-tailed Student's *t* test). Top right, immunostaining of representative paraffin sections from perichondrial groove of Ranvier region of Ctsk-KO and control mice. Note the decreased number of p-Erk⁺ cells (75.4% in Ctsk-control versus 32.2% in Ctsk-KO; $n = 3$ mice). Bottom, note the increased *Ihh* expression but unchanged p-Akt staining in Ctsk-KO, compared with control, mice. **b**, Top left, immunoblot showing Shp2 in ATDC5 knockdown (KD) cells, stably expressing shRNAs against mouse *Ptpn11* (ATDC5-KD1, ATDC5-KD2) or scrambled control hairpin. Top right, Representative blot showing that Shp2 deficiency decreases Erk activation in response to Fgf18; data from multiple experiments ($n = 3$) showing p-Erk levels (compared with control at 5 min, mean \pm s.d.; $P < 0.05$, two-tailed Student's

t test) are quantified below (bottom right). qRT-PCR (bottom left) shows increased *Ihh* and *Pthrp* expression in Shp2-deficient ATDC5 cells (mean \pm s.d.; $n = 3$, * $P < 0.05$, two-tailed Student's *t* test). **c**, FGFR (PD173074, 10 nM) or MEK (UO126, 1 μ M) inhibitor treatment (FGFRi and UO, respectively) of parental ATDC5 cells enhances *Ihh* and *Pthrp* expression, as shown by qRT-PCR (mean \pm s.d.; $n = 3$, * $P < 0.05$, two-tailed Student's *t* test). **d**, Faxitron radiographs showing that hedgehog pathway blockade following administration of the SMOi (100 μ g g⁻¹ body weight) to Ctsk-KO mice ameliorates tumour formation, compared with vehicle control (0.5% methylcellulose)-treated mice. Images of representative posterior paws (i–iv) and knees (v–viii) taken before (i, iii, v, vii) and after treatment with vehicle (ii, vi) or SMOi (iv, viii) for 4 weeks. Note continued development of exostoses and enchondromas in vehicle-treated mice, and their amelioration in SMOi-treated group (arrows). Also see Supplementary Figs 4–7 and Supplementary Video 1.

mice (Fig. 4d and Supplementary Figs 4–7) and markedly improved their mobility (Supplementary Video 1), without apparent effects on overall growth rate (Supplementary Fig. 8). Importantly, SMOi levels in treated mice were adequate to suppress *Ihh* target gene expression in exostoses (Supplementary Fig. 7b).

Our findings strongly suggest that metachondromatosis results from loss of SHP2, specifically in CCPs, a heretofore poorly characterized population within the perichondrial groove of Ranvier, which is believed to function as a stem-cell niche for joints¹⁶ and a reservoir for the germinal layer cells of the growth plate²⁴. Cells within the groove of Ranvier express high levels of FGFR3 (ref. 25), and their removal prevents longitudinal bone growth²⁶. Emerging evidence shows that groove of Ranvier cells can migrate into articular cartilage¹⁶, implicating them in maintaining cartilage homeostasis and possibly in degenerative joint diseases, such as osteoarthritis. Indeed, in lineage-tracing studies of normal mice, we noticed YFP⁺ cells migrating towards articular cartilage (Supplementary Fig. 9, arrows, and data not shown). On the basis of our mouse metachondromatosis model, we propose that SHP2, acting downstream of FGFR3 and upstream of the RAS/ERK pathway, regulates CCP proliferation and chondrogenic

differentiation. Consequently, *PTPN11* deficiency in these cells promotes excessive proliferation, chondrogenic differentiation and cartilage tumours.

Metachondromatosis is associated with heterozygous inactivating mutations in *PTPN11*, yet Ctsk-control mice are normal, whereas Ctsk-KO mice exhibit metachondromatosis-like features. Although *PTPN11* gene dosage effects could differ in mouse and man (and thus 50% reduction in SHP2 level might cause metachondromatosis in humans but not in mice), we think it is more likely that loss of the remaining *PTPN11* allele (for example, by loss of heterozygosity or silencing) is required to cause cartilage tumours in metachondromatosis. If so, then unlike its oncogenic role in juvenile myelomonocytic leukaemia, other hematologic malignancies and solid tumours^{1,2}, *PTPN11* is a tumour suppressor in cartilage. Liver-specific *Ptpn11* deletion reportedly results in hepatocellular carcinoma²⁷. However, we have not seen liver tumours in our *Ptpn11* conditional knockout mice crossed to the same Cre line (F.H. & B.G.N., manuscript in preparation), nor is *PTPN11* mutated in human hepatocellular carcinoma. Moreover, our biochemical and pharmacological analysis, together with previous studies, provide a parsimonious and attractive explanation for the

apparently paradoxical pro- and anti-oncogenic effects of *PTPN11*. In both cases, SHP2 is a critical regulator of ERK. The activating *PTPN11* mutations associated with cancer promote proliferation and survival, at least in part via increased ERK activation. Similarly, overexpression or increased activation of normal SHP2 binding proteins such as GAB2, or the presence of pathologic SHP2 binding proteins such as *Helicobacter pylori* CagA²⁸, can hyperactivate ERK and contribute to various malignancies. Conversely, SHP2 deficiency is oncogenic in CCPs because in these cells, ERK normally represses the expression of the growth stimulator IHH (which, in turn, stimulates PTHRP production). Future studies should focus on better defining the properties of CCPs, determining whether *PTPN11* also acts as a tumour suppressor in other cartilage neoplasms, including chondrosarcoma, and most importantly, on testing the effects of smoothed inhibition in metachondromatosis patients. Finally, given our proposed mechanism of metachondromatosis pathogenesis, our results call for caution in the long-term use of MEK or ERK inhibitors.

METHODS SUMMARY

Ptpn11 floxed (*Ptpn11*^{f/f})¹⁰, *cathepsin K-Cre* (*Ctsk-Cre*)¹², *Rosa26-LSL-lacZ* (*R26-LSL-lacZ*)²⁹, and *Rosa26-LSL-YFP* (*R26-LSL-YFP*)³⁰ Cre reporter mice were on C57BL/6 background. PCR genotyping was performed as described^{10,12,29,30}; conditions are available from W.Y. Animal studies were approved by the Institutional Animal Care and Use Committee at Rhode Island Hospital. Mice of both genders were used for this study. Antibodies and reagents are detailed in Methods. CCPs isolated from epiphyseal cartilage of 2-week-old *Ctsk-control*;YFP and *Ctsk-KO*;YFP mice (detailed in Methods) were analysed by flow cytometry or subjected to multi-lineage differentiation assays. For flow cytometry, cells were stained with fluorescence-labelled antibodies, and analysed on a BD LSR II flow cytometer using FlowJo software (TreeStar). YFP⁺ cells were purified by using a BD Influx cell sorter (BD Bioscience). ATDC5 cells stably expressing mouse *Ptpn11* shRNAs or a scrambled control were generated in pSuper(retro)/puro (Oligoengine). RNA was extracted from cells or laser-dissected lesions using RNeasy (Qiagen), complementary DNA was synthesized using iScript (Bio-Rad), and qRT-PCR was performed with the iQ SYBR Green kit. Values were normalized to *Gapdh* levels, and are expressed as fold-change over control. Primer sequences are available from W.Y.. Femurs, tibiae and paws were fixed in 4% paraformaldehyde, decalcified in 0.5 M EDTA, and sections (5 µm) were stained with haematoxylin and eosin, Alcian Blue or Safranin O. Immunohistochemistry was performed using peroxidase-coupled secondary antibodies, with diaminobenzidine as the substrate. X-gal staining was performed as described¹². Digital imaging was performed using Faxitron (plain films) and desktop microcomputed tomographic (µ-CT40, Scanco Medical) systems. The number of exostoses was quantified from these images. Immunoblotting and detection by enhanced chemiluminescence (Amersham) were performed as described¹⁰. Differences between groups were evaluated by Student's *t* test, with *P* < 0.05 considered significant.

Full Methods and any associated references are available in the online version of the paper.

Received 3 May 2012; accepted 21 June 2013.

Published online 17 July 2013.

1. Neel, B. G., Chan, G. & Dhanji, S. in *Handbook of Cell Signaling* Vol. 2 (eds Bradshaw, R. A. & Dennis, E. A.) Ch. 98, 771–809 (2009).
2. Grossmann, K. S., Rosario, M., Birchmeier, C. & Birchmeier, W. The tyrosine phosphatase Shp2 in development and cancer. *Adv. Cancer Res.* **106**, 53–89 (2010).
3. Bowen, M. E. *et al.* Loss-of-function mutations in *PTPN11* cause metachondromatosis, but not Ollier disease or Maffucci syndrome. *PLoS Genet.* **7**, e1002050 (2011).
4. Sobreira, N. L. *et al.* Whole-genome sequencing of a single proband together with linkage analysis identifies a Mendelian disease gene. *PLoS Genet.* **6**, e1000991 (2010).
5. Bovée, J. V., Hogendoorn, P. C., Wunder, J. S. & Alman, B. A. Cartilage tumours and bone development: molecular pathology and possible therapeutic targets. *Nature Rev. Cancer* **10**, 481–488 (2010).
6. Pannier, S. & Legeai-Mallet, L. Hereditary multiple exostoses and enchondromatosis. *Best Pract. Res. Clin. Rheumatol.* **22**, 45–54 (2008).
7. Pansuriya, T. C., Kroon, H. M. & Bovee, J. V. Enchondromatosis: insights on the different subtypes. *Int. J. Clin. Exp. Pathol.* **3**, 557–569 (2010).

8. Tartaglia, M., Gelb, B. D. & Zenker, M. Noonan syndrome and clinically related disorders. *Best Pract. Res. Clin. Endocrinol. Metab.* **25**, 161–179 (2011).
9. Saxton, T. M. *et al.* Abnormal mesoderm patterning in mouse embryos mutant for the SH2 tyrosine phosphatase Shp-2. *EMBO J.* **16**, 2352–2364 (1997).
10. Yang, W. *et al.* An Shp2/SFK/Ras/Erk signaling pathway controls trophoblast stem cell survival. *Dev. Cell* **10**, 317–327 (2006).
11. Clausen, B. E., Burkhardt, C., Reith, W., Renkawitz, R. & Forster, I. Conditional gene targeting in macrophages and granulocytes using LysMcre mice. *Transgenic Res.* **8**, 265–277 (1999).
12. Nakamura, T. *et al.* Estrogen prevents bone loss via estrogen receptor α and induction of Fas ligand in osteoclasts. *Cell* **130**, 811–823 (2007).
13. Dodds, R. A., Connor, J. R., Drake, F., Feild, J. & Gowen, M. Cathepsin K mRNA detection is restricted to osteoclasts during fetal mouse development. *J. Bone Miner. Res.* **13**, 673–682 (1998).
14. Langenskiöld, A. Role of the ossification groove of Ranvier in normal and pathologic bone growth: a review. *J. Pediatr. Orthop.* **18**, 173–177 (1998).
15. Shapiro, F., Holtrop, M. E. & Glimcher, M. J. Organization and cellular biology of the perichondrial ossification groove of ranvier: a morphological study in rabbits. *J. Bone Joint Surg. Am.* **59**, 703–723 (1977).
16. Karlsson, C., Thormemo, M., Henriksson, H. B. & Lindahl, A. Identification of a stem cell niche in the zone of Ranvier within the knee joint. *J. Anat.* **215**, 355–363 (2009).
17. Goldring, M. B., Tsuchimochi, K. & Ijiri, K. The control of chondrogenesis. *J. Cell. Biochem.* **97**, 33–44 (2006).
18. Hopyan, S. *et al.* A mutant PTH/PTHrP type I receptor in enchondromatosis. *Nature Genet.* **30**, 306–310 (2002).
19. Tiet, T. D. *et al.* Constitutive Hedgehog signaling in chondrosarcoma up-regulates tumor cell proliferation. *Am. J. Pathol.* **168**, 321–330 (2006).
20. Liu, Z., Xu, J., Colvin, J. S. & Ornitz, D. M. Coordination of chondrogenesis and osteogenesis by fibroblast growth factor 18. *Genes Dev.* **16**, 859–869 (2002).
21. Ohbayashi, N. *et al.* FGF18 is required for normal cell proliferation and differentiation during osteogenesis and chondrogenesis. *Genes Dev.* **16**, 870–879 (2002).
22. Kronenberg, H. M. PTHrP and skeletal development. *Ann. NY Acad. Sci.* **1068**, 1–13 (2006).
23. Murakami, S. *et al.* Constitutive activation of MEK1 in chondrocytes causes Stat1-independent achondroplasia-like dwarfism and rescues the *Fgf3*-deficient mouse phenotype. *Genes Dev.* **18**, 290–305 (2004).
24. Fenichel, I., Evron, Z. & Nevo, Z. The perichondrial ring as a reservoir for precartilaginous cells. *In vivo* model in young chicks' epiphysis. *Int. Orthop.* **30**, 353–356 (2006).
25. Robinson, D. *et al.* Fibroblast growth factor receptor-3 as a marker for precartilaginous stem cells. *Clin. Orthop. Relat. Res.* **S163–S175** (1999).
26. Rodriguez, J. I., Delgado, E. & Paniagua, R. Changes in young rat radius following excision of the perichondrial ring. *Calcif. Tissue Int.* **37**, 677–683 (1985).
27. Bard-Chapeau, E. A. *et al.* *Ptpn11/Shp2* acts as a tumor suppressor in hepatocellular carcinogenesis. *Cancer Cell* **19**, 629–639 (2011).
28. Hatakeyama, M. Oncogenic mechanisms of the *Helicobacter pylori* CagA protein. *Nature Rev. Cancer* **4**, 688–694 (2004).
29. Soriano, P. Generalized lacZ expression with the ROSA26 Cre reporter strain. *Nature Genet.* **21**, 70–71 (1999).
30. Srinivas, S. *et al.* Cre reporter strains produced by targeted insertion of *EYFP* and *ECFP* into the ROSA26 locus. *BMC Dev. Biol.* **1**, 4 (2001).

Supplementary Information is available in the online version of the paper.

Acknowledgements We thank S. Kato for *Ctsk-Cre* mice, A. Craft for review of the manuscript, X. Wang and P. Monfils for help with histology and J. Cao for helping with μ -CT analysis. This publication was made possible by the National Institutes of Health (NIH) and the National Institute for General Medicine Sciences (NIGMS) grant no. 8P20GM103468. This work was also funded by NIH R21AR57156 (to W.Y.) and R37CA49152 (to B.G.N.), the Rhode Island Hospital Orthopaedic Foundation and a grant from the Pediatric Orthopaedic Society of North America and the Orthopaedic Research and Education Foundation (to W.Y.). B.G.N. is a Canada Research Chair, Tier 1, and is also supported in part by the Ontario Ministry of Health and Long Term Care and the Princess Margaret Cancer Foundation.

Author Contributions W.Y. and B.G.N. conceived the project. J.W., D.M., H.L. and W.Y. carried out most of the experiments. M.D. and W.Y. conducted FACS sorting and analysis. H.L. performed the SMOi animal treatment experiment. J.W. performed gene expression and western blot analysis. M.D. and J.W. carried out bone marrow transplantation experiments with the advice of P.J.Q. M.D., H.L. and W.Y. performed CPC multi-lineage differentiation assays. Q.W. and R.T. performed histological staining and data interpretation. Q.C. and M.G.E. provided technical and intellectual support. W.Y. and B.G.N. analysed the data and wrote the manuscript with the help of all authors.

Author Information Reprints and permissions information is available at www.nature.com/reprints. The authors declare competing financial interests: details are available in the online version of the paper. Readers are welcome to comment on the online version of the paper. Correspondence and requests for materials should be addressed to W.Y. (wyang@lifespan.org).

METHODS

Ptpn11 floxed (*Ptpn11^{fl}*)¹⁰, *cathepsin K-Cre* (Ctsk-Cre)¹², *Rosa26-LSL-lacZ* (*R26-LSL-lacZ*)²⁹, and *Rosa26-LSL-YFP* (*R26-LSL-YFP*)³⁰ Cre reporter mice were on C57BL/6 background.

Antibodies and reagents. The following antibodies were purchased: monoclonal anti-p-tyrosine (4G10) was from Millipore; polyclonal antibodies against p-Erk1/2, Erk2, p-Akt(Ser 473), Akt, Shp2, p-Stat1 (Tyr 701) and Stat1 were from Cell Signaling; antibodies against Ihh, Col2 α 1 and Col10 α 1 were from Santa Cruz Biotechnology and Abcam, respectively; fluorescence-labelled antibodies against CD31, CD44, CD45, CD90 and CD166 were purchased from eBioscience; and antibodies against Stro-1 and jagged 1 were purchased from Invitrogen and EpiTomics, respectively. Alexa 488-labelled goat anti-rabbit IgG and Alexa 594-labelled anti-rabbit and anti-mouse IgG were purchased from Invitrogen. Fgf18 was purchased from PeprroTech. UO126 and PD173074 were from Calbiochem and Selleckbio, respectively. PF-04449913 was kindly provided by Pfizer. Alcian Blue, Alizarin Red S and Oil Red O staining solutions were purchased from Poly Scientific.

Cell isolation and culture. To isolate YFP⁺ CCPs, epiphyseal cartilage was dissected from 2-week-old Ctsk-control; YFP and Ctsk-KO; YFP mice, and digested with hyaluronidase (2.5 mg ml⁻¹, Sigma) and trypsin-EDTA (0.25%, Invitrogen) to remove soft tissues, and then with collagenase D (2.5 mg ml⁻¹, Roche) for 4–6 h to release all cartilage cells. After washing in PBS, cells were stained with fluorescence-labelled antibodies (using concentrations recommended by the manufacturers), and analysed by flow cytometry, or YFP⁺ cells were purified by FACS and placed in short-term cultures (3–4 days) in murine mesenchymal culture medium (StemCell Technologies) containing 10% FBS.

Parental ATDC5 cells were obtained from C. Phornphutkul (Brown University) and cultured in complete DMEM/F12 medium (1:1) (Invitrogen), as described³¹. shRNAs against mouse *Ptpn11* (KD1: 5'-GATTCAGAACACTGGGACTTCAAGAGATCCCCAGTGTCTGAATC-3'; KD2: 5'-GAGTAACCCTGGAGACTTCTTCAAGAGAGAAGTCTCCAGGGTTACTC-3'), or a scrambled control for KD1 (5'-TAGTACAAGTCCAAGCGGCTTCAAGAGA GCCGCTGGACTTGTACTA-3'), were introduced into the retroviral vector pSuper(retro)/puro (Oligoengine). Viral supernatants were collected from 293T cells co-transfected with each retroviral vector and Ecopac, and used to infect ATDC5 cells, which were then selected with puromycin³².

Differentiation assays. CCPs (~2 × 10⁴), purified by FACS (for YFP) from 10–14-day-old *Ctsk-R26-LSL-YFP* reporter mice, were cultured in differentiation medium for chondrocytes (DMEM with 10% FBS, 0.1 μ M dexamethasone, 0.1 mM ascorbic acid, 10 mM glycerol 2-phosphate, 1 ng ml⁻¹ TGF- β 1), adipocytes (DMEM with 10% FBS, 1 μ M dexamethasone, 0.5 mM 3-isobutyl-1-methylxanthine (IBMX), 10 μ g ml⁻¹ insulin), or osteoblasts (DMEM with 10% FBS, 0.1 μ M dexamethasone, 0.2 mM ascorbic acid, 10 mM glycerol-2-phosphate, 10 ng ml⁻¹ rhMBP2), respectively. After culturing for 2 (adipogenic or chondrogenic differentiation) or 3 weeks (osteogenesis), cells were fixed and stained with Alcian Blue, Oil Red O or Alizarin Red to visualize the formation of cartilage, fat, and bone tissue, respectively.

qRT-PCR. RNA was extracted from cultured cells or cartilage lesions enriched by laser-capture using the RNeasy kit (Qiagen). cDNA was synthesized using iScriptcDNA Synthesis Kit (Bio-Rad), and qRT-PCR was performed by using the iQ SYBR Green qPCR kit. All values were normalized to *Gapdh* levels, and qRT-PCR data were expressed as fold-increases compared with controls. Primer sequences and PCR conditions are available from W.Y. upon request.

Flow cytometry and FACS. Epiphyseal cartilage cells were stained with fluorescence-labelled antibodies, as described³³, and analysed on a BD LSR II flow cytometer. YFP⁺ cells were purified by FACS using a BD Influx cell sorter (BD Bioscience). Flow cytometric data were analysed with FlowJo software (TreeStar).

Histology. Ctsk-control and Ctsk-KO mice were euthanized at the indicated ages, and femurs, tibiae and paws were removed and fixed in 4% PFA overnight at 4 °C. Postnatal skeletal tissues were decalcified in 0.5 M EDTA before embedding. Tissue sections (5 μ m) were stained with haematoxylin and eosin, Alcian blue or Safranin O. Immunofluorescence staining was carried out using secondary antibodies conjugated to the indicated fluorophores at concentrations recommended by their manufacturers. Immunohistochemistry was performed using fluorescence- or peroxidase-coupled anti-rabbit, -mouse or -goat secondary antibodies, as per the manufacturer's instructions, with diaminobenzidine serving as the substrate. X-gal staining was performed as described¹².

Drug treatment. Two trials were performed using the smoothened inhibitor PF-04449913. In a pilot study, groups (five mice per each group) of knockout mice were treated with SMOi (100 μ g g⁻¹ body weight) or vehicle control (0.5% methylcellulose), beginning at 5 weeks of age (at which time early lesions were present) and continuing for the succeeding 4 weeks. Mice were randomized by alternate assignment to control (vehicle) or drug treatment arms. The pilot experiment showed a significant difference in number of exostoses (assessed radiographically) in the SMOi group, and led to a second study (again involving five mice each) to confirm these findings and also assess additional parameters (μ -CT, histology, gene expression). Two mice (one each from control and experimental groups, respectively) died for unknown reasons during the second trial, and were excluded from the analysis because they were removed from cages and could not be recovered. All surviving mice from both studies were included in the analyses shown in the text.

Microcomputed tomography (μ -CT) and X-ray analysis. X-ray images of the entire skeleton, knees, metatarsals and phalanges were obtained immediately after euthanasia by using a Faxitron X-ray system (Wheeling). After fixation in 4% PFA, μ -CT images of skeletal tissues were scanned with a desktop microcomputer graphic imaging system (μ CT40, Scanco Medical AG). The number of exostoses was measured from these radiographic images, as indicated in the figure legends. For these studies, mice were assigned a code number by the animal technician, and blinded quantification was carried out by W.Y.

Immunoblotting. Cells were lysed in modified NP-40 buffer (0.5% NP-40, 150 mM NaCl, 1 mM EDTA, 50 mM Tris (pH 7.4)), supplemented with a protease inhibitor cocktail (1 mM PMSF, 1 mM NaF, 1 mM sodium orthovanadate, 10 mg ml⁻¹ aprotinin, 0.5 mg ml⁻¹ antipain and 0.5 mg ml⁻¹ pepstatin), as described¹⁰. For immunoblotting, cell lysates (10–50 μ g) were resolved by SDS-PAGE, transferred to polyvinylidene difluoride membranes, and incubated with primary antibodies for 2 h or overnight at 4 °C (according to the manufacturer's instructions), followed by horseradish peroxidase-conjugated secondary antibodies. Detection was by enhanced chemiluminescence (Amersham). Signals were quantified using NIH ImageJ.

Statistical analysis. Differences between groups were evaluated by Student's *t* test. A *p* value of <0.05 was considered significant. For all of these experiments, between-group variances were similar and data were symmetrically distributed. All analyses were performed by using Excel (Microsoft) and Prism 3.0 (GraphPad).

- Hidaka, K. *et al.* Involvement of the phosphoinositide 3-kinase/protein kinase B signaling pathway in insulin/IGF-I-induced chondrogenesis of the mouse embryonal carcinoma-derived cell line ATDC5. *Int. J. Biochem. Cell Biol.* **33**, 1094–1103 (2001).
- Mohi, M. G. *et al.* Prognostic, therapeutic, and mechanistic implications of a mouse model of leukemia evoked by Shp2 (*PTPN11*) mutations. *Cancer Cell* **7**, 179–191 (2005).
- Pretzel, D. *et al.* Relative percentage and zonal distribution of mesenchymal progenitor cells in human osteoarthritic and normal cartilage. *Arthritis Res. Ther.* **13**, R64 (2011).

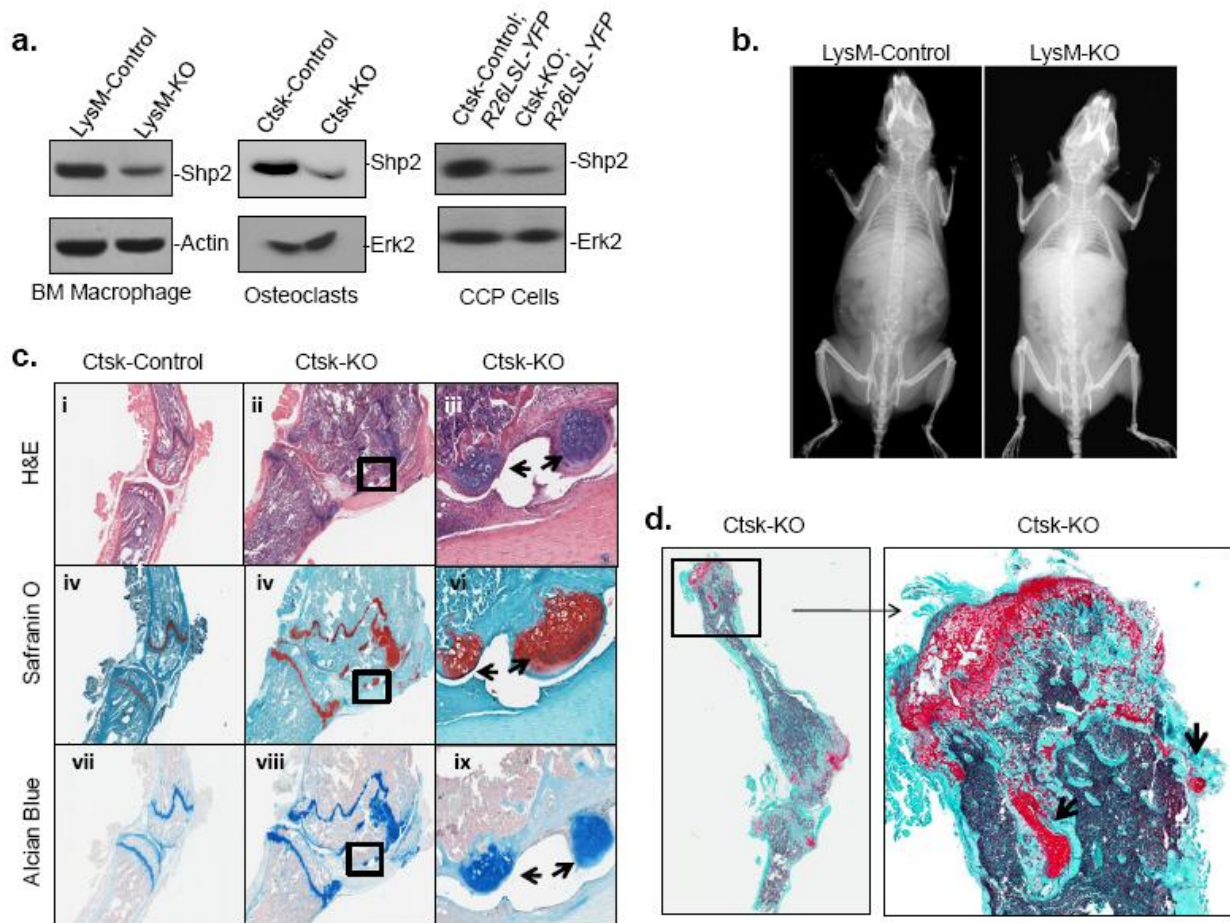


Figure S1 | **a**, Immunoblots showing Shp2 levels in bone marrow-derived macrophages (left), osteoclasts (middle), and YFP⁺ perichondrial cells (CCPs) (right) from Ctsk-Control/R26LSL-YFP and KO/R26LSL-YFP mice, as indicated; Erk2 levels serve as a loading control. **b**, Representative Faxitron radiographs demonstrating increased bone mineral density in LysM-KO mice compared with Controls, but no exostoses or joint deformation. Similar results were obtained in 5 additional mice. **c**, H&E- (i-iii), Safranin O- (iv-vi) and Alcian blue (vii-ix) staining of sagittal sections of knee joints from 12-week-old Ctsk-Control (i, iv, vii) and Ctsk-KO (ii, iii, v, vi, viii, ix) mice. Images iii, vi & ix are magnified views (10x) of the boxed areas in ii, v, and viii, respectively. Note exostoses (arrows) in Ctsk-KO mice. Compared with Controls, Ctsk-KO mice have markedly enlarged distal femurs and proximal tibiae and elongated metaphyses with a broad and coast shape-like growth plate cartilage (ii, v, viii). Newly forming cartilage masses are seen readily at the epiphyses (iii, vi, ix). **d**, Safranin O stain showing enchondromas (arrows) in tubular bones of Ctsk-KO mice. Data in panels a-d are from single animals; similar results were obtained from analyses of at least 4 additional mice/genotype.

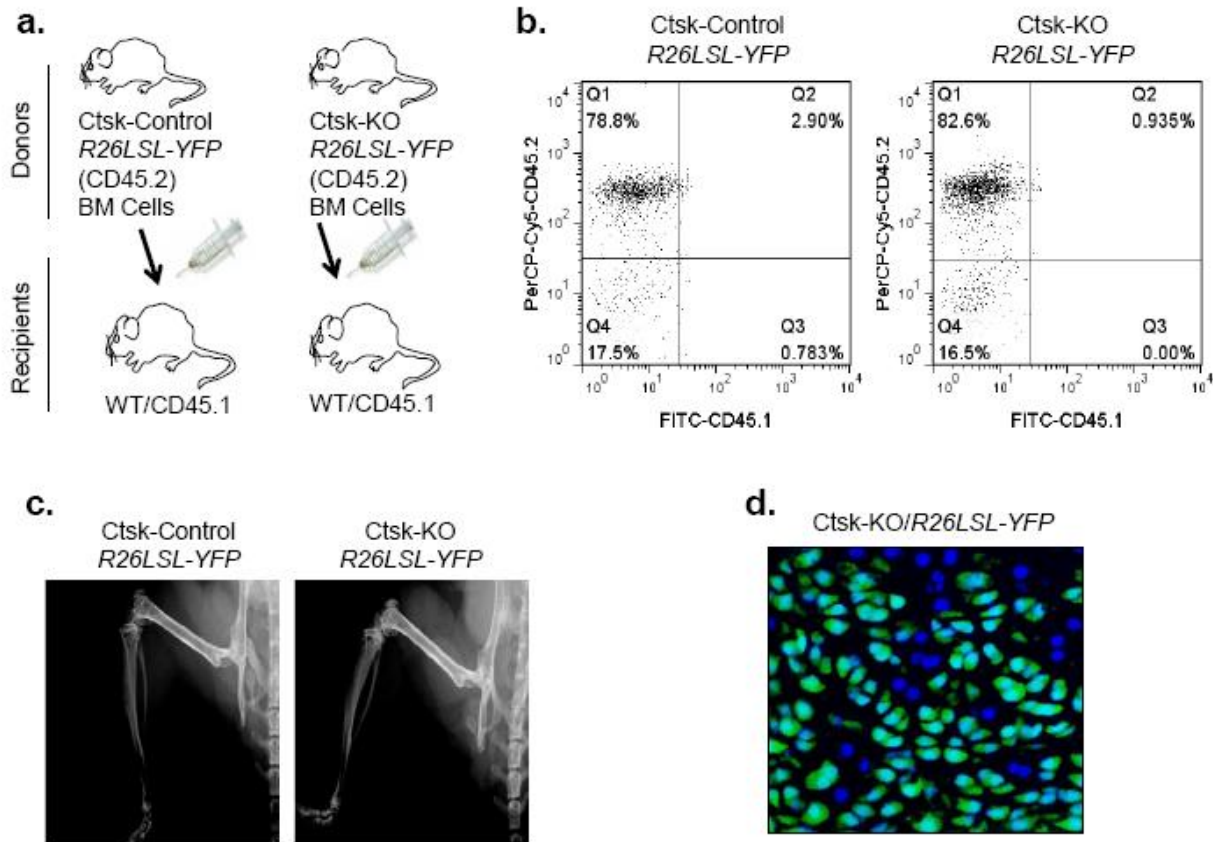


Figure S2 | a, Scheme of bone marrow transplant experiments used to examine the role of osteoclasts (or other bone marrow-derived cells) in skeletal pathogenesis in Ctsk-KO mice. **b**, Flow cytometric analysis of peripheral blood showing high engraftment of donor BM cells from Ctsk-KO/R26LSL-YFP and Ctsk-Control/R26LSL-YFP (C57BL/6; CD45.2) mice in lethally irradiated recipients (B6.SJL; CD45.1). Tail vein bleeding was performed 12 weeks post-BMT. A representative flow blot is shown; similar results were obtained in 6 other recipients. **c**, Faxitron radiographs showing that recipients of Ctsk-KO, but not Ctsk-Control, bone marrow have increased bone mineral density, but do not develop exostoses after ≥ 12 months of observation; data are from one of seven independent recipients. **d**, Fluorescence micrograph demonstrating that the majority of the cells (70-90%) in exostoses are YFP⁺ in Ctsk-KO/R26LSL-YFP reporter mice. Exostoses from the rear paws of 8-week-old Ctsk-KO/R26LSL-YFP mice were fixed and sectioned to visualize YFP⁺ cells. Data shown are representative of 4 mice/genotype.

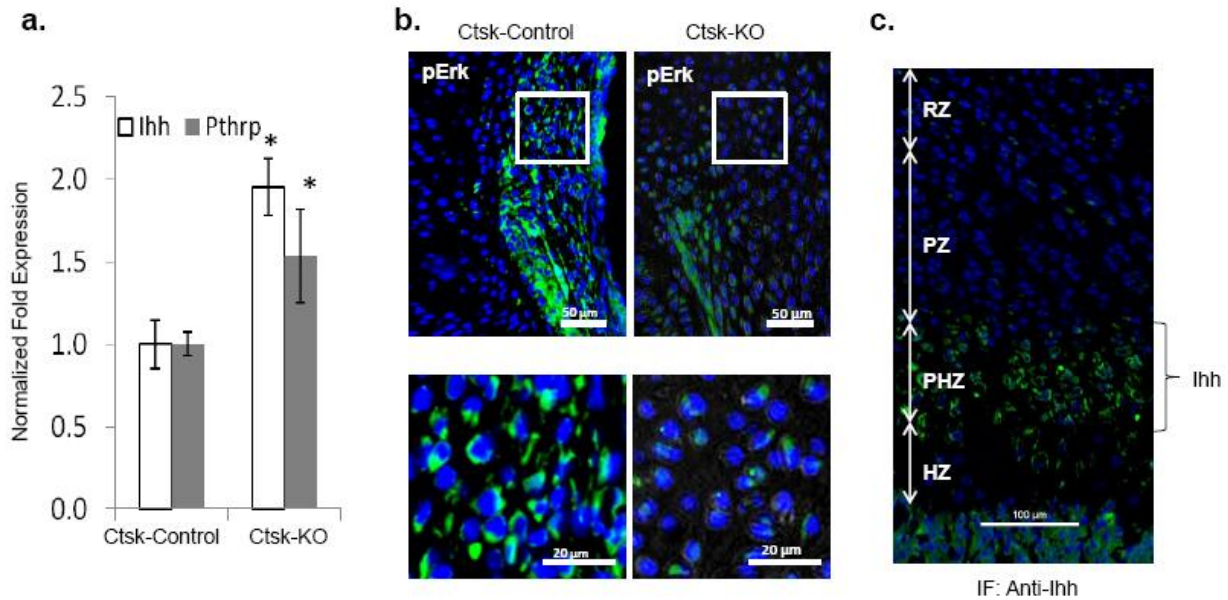


Figure S3 | a. qRT-PCR analysis showing increased *Ihh* and *Pthrp* expression in laser-captured cartilaginous cells from exostoses from 3 mice, compared with normal growth plate cartilage cells (mean \pm S.D., * p <0.05, 2-tailed Student's t test). **b.** High magnification images showing decreased percentage of p-Erk-positive cells in the Groove of Ranvier of Ctsk-KO mice compared with Ctsk-Control mice (Percentage of nuclei that are pErk+ in the boxed area from 3 mice: 75.4% in Ctsk-Control vs. 32.2% in Ctsk-KO, p <0.002, 2-tailed Student's t test); **c.** Fluorescence micrograph showing *Ihh* immunostaining in growth plate cartilage from 2-week-old wild type mice; note that under these conditions only pre-hypertrophic chondrocytes are positive for *Ihh* expression, indicating that the *Ihh* immunostaining conditions are specific.

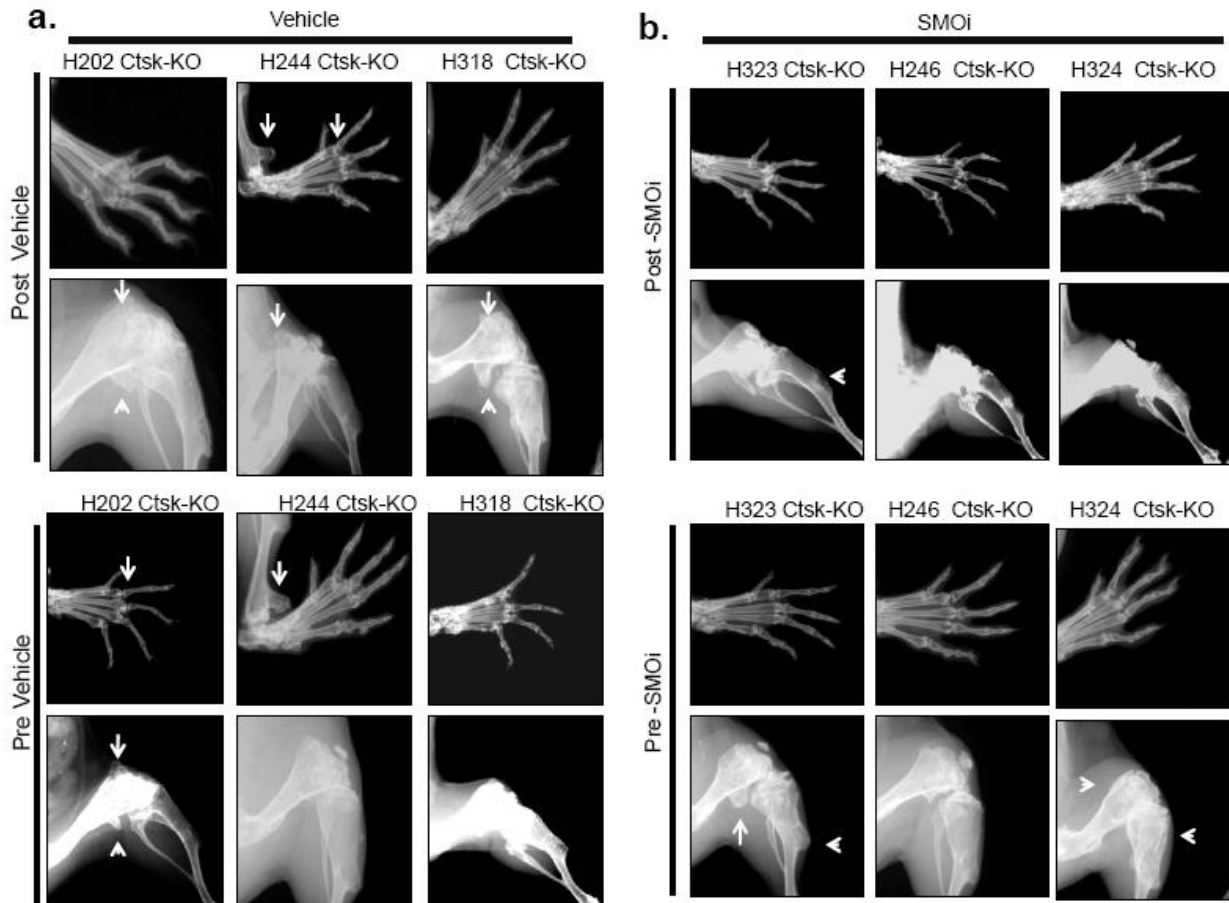


Figure S4 | Representative Faxitron radiographs of Ctsk-KO mice (from total n=9) treated with the Smoothed inhibitor (SMOi) PF-04449913 (100 μ g/g body weight) or Vehicle control (0.5% methylcellulose) by daily gavage beginning at post-natal week 5 and continuing to week 9, when mice were sacrificed. Note the reduced number and size of exostoses (arrows) in SMOi-, but not Vehicle- treated Ctsk-KO mice (also see Fig. S5).

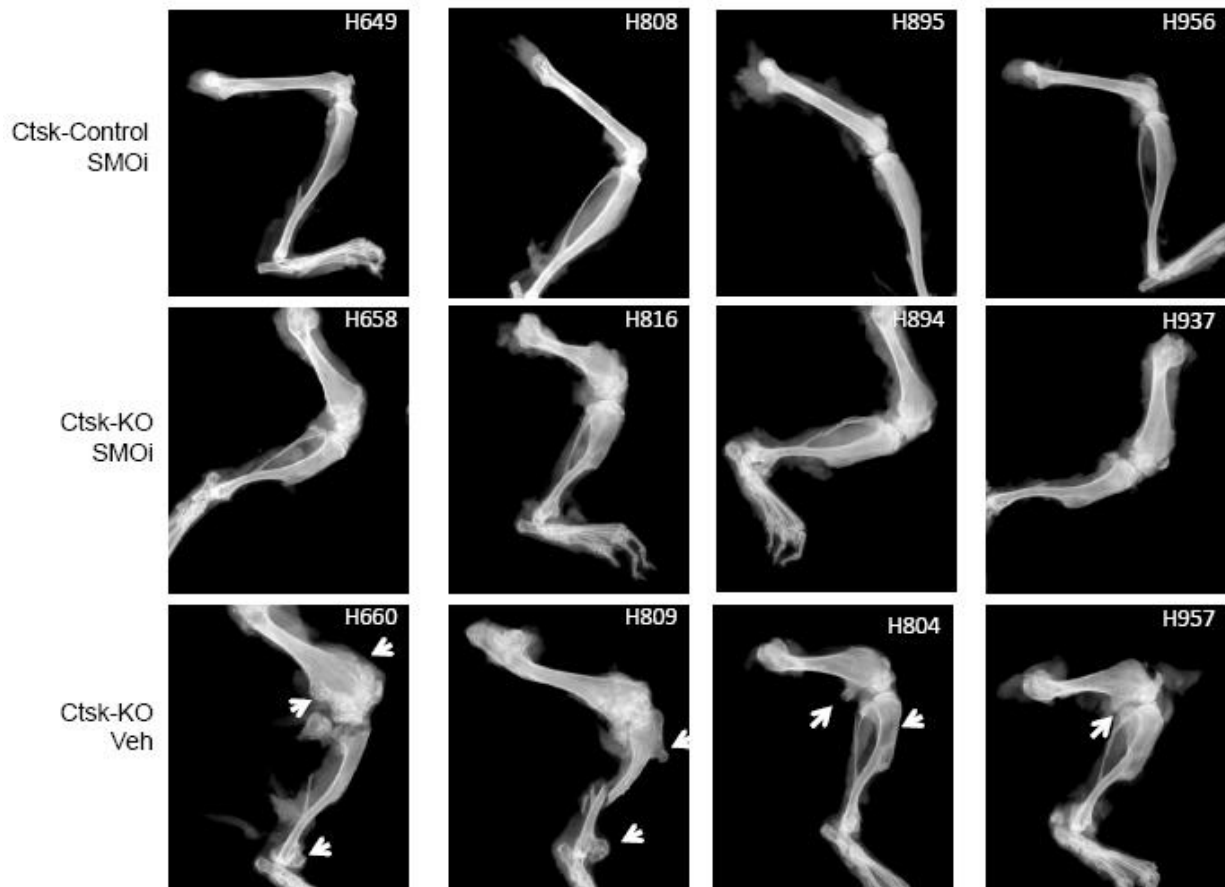


Figure S5 I Additional Faxitron images of femurs and tibiae taken from 9-week-old Ctsk-Control and Ctsk-KO mice post-SMOi or -Vehicle treatment. Note the readily observed exostoses in the metaphases of Ctsk-KO mice (arrows) treated with Vehicle but not SMOi.

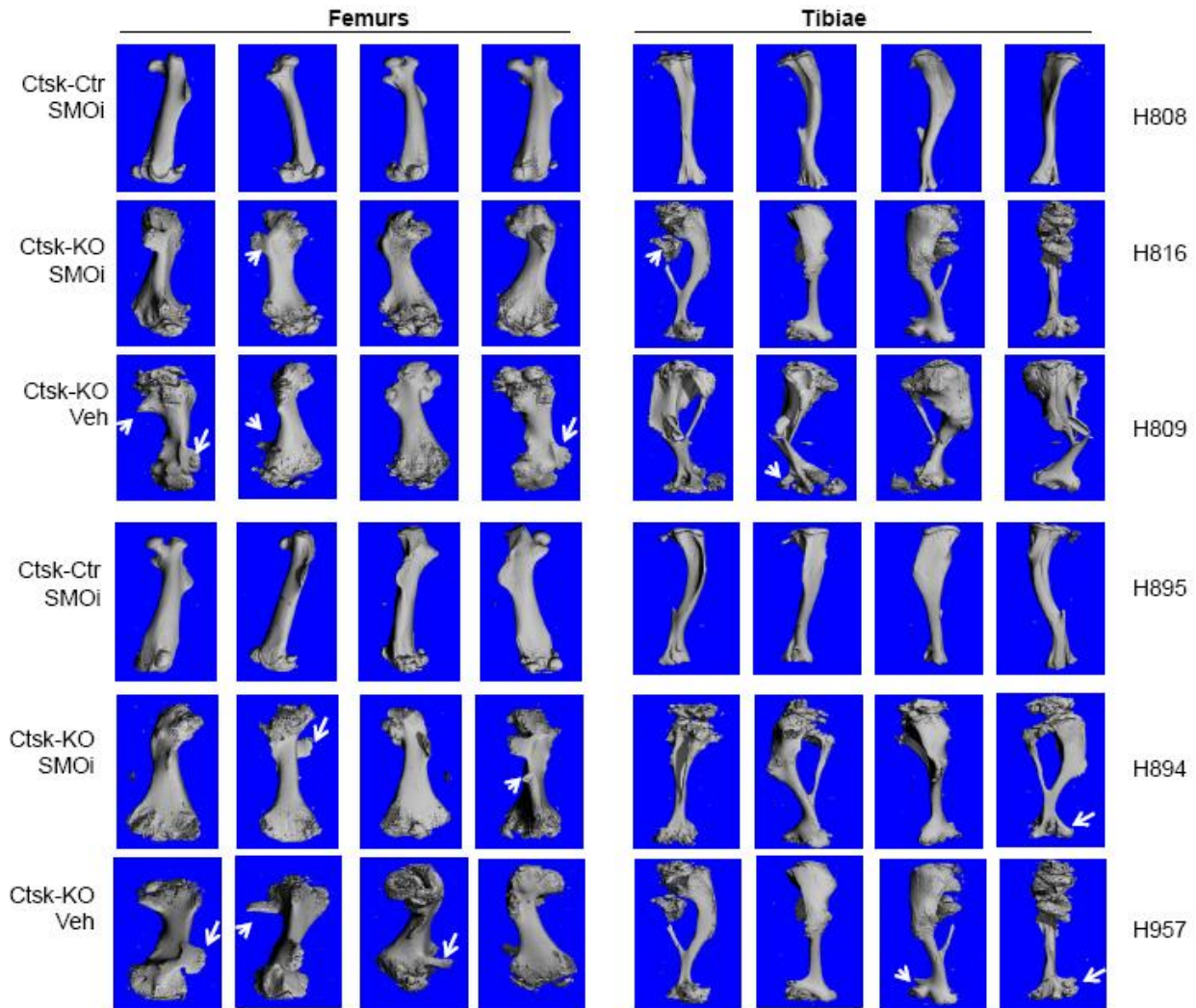


Figure S6 | a. Representative μ -CT images of Ctsk-KO mice treated with Vehicle or Smoothed inhibitor (SMOi), as described in Fig. S3 (from total $n=9$ each treatment). Note the decrease in number and size of exostoses (arrows) in treated mice; see Fig. S7 for quantification.

a.

Average number of exostoses (+SD)			
Treatment	Vehicle	SMOi	(<i>p</i>)
Posterior Paw	3.88±0.69	2.94±0.80	<0.012*
Femur & Tibiae	3.83±1	3.05±0.53	<0.027*

Exostoses formed at rear limbs post-vehicle treatment

N	1	2	3	4	5	6	7	8	9	Average
Posterior Paw	4.5	3.5	3.5	4	4	3	4.5	3	5	3.88889
Femur & Tibiae	4	3	5	4.5	3	5	4	4	2	3.83333

Exostoses formed at rear limbs post-SMOi treatment

N	1	2	3	4	5	6	7	8	9	Average
Posterior Paw	3	4	3.5	2	4	2	3	2	3	2.94444
Femur & Tibiae &	3	3.5	3	4	3	3	3	3	2	3.05556

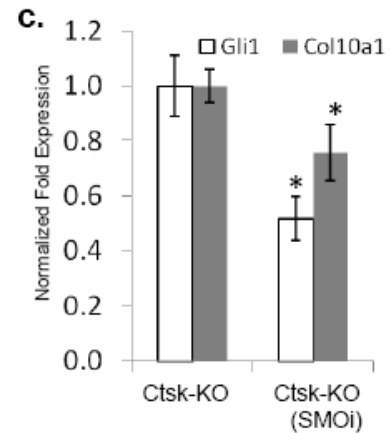
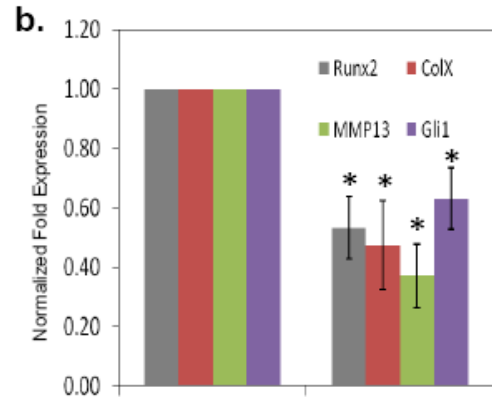


Figure S7 | a. Number of exostoses in Ctsk-KO mice (from n=9 each condition) post-treatment with Vehicle or Smoothened inhibitor (SMOi), as described in Fig. S6. Note the decrease in average number of exostoses/per paw, knee, and tibiae. Significance was assessed by 2-tailed Student’s *t* test. Bottom panel shows numbers of exostoses in individual mice used to calculate the averages in top panel. **b-c.** qRT-PCR showing that administration of the Smoothened inhibitor PF-04449913 (SMOi) by gavage to wild type mice for 1 week blunts the expression of *Col2a1*, *Col10a1*, *Mmp13* and *Gli1* in epiphyseal cartilage (**b**), whereas SMOi administration to Ctsk-KO mice for 4 weeks decreases the expression of *Gli1* and *Col10a1* in exostotic lesions, compared with vehicle controls (**c**). Data are presented as mean±S.D. (n=3, **p*<0.05, unpaired Student’s *t* test).

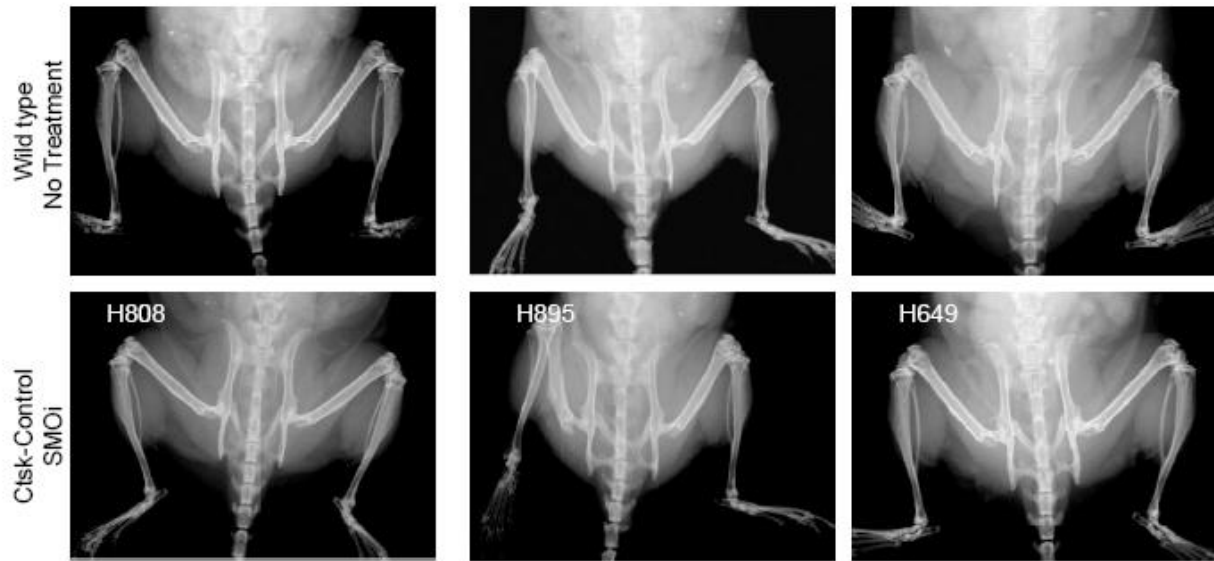


Figure S8 | Faxitron images taken from 9-week-old wild type and Ctsk-Control mice treated with SMOi, as described in **Methods**. No apparent skeletal retardation was apparent in SMOi-treated group compared wild type controls (n=3 each).

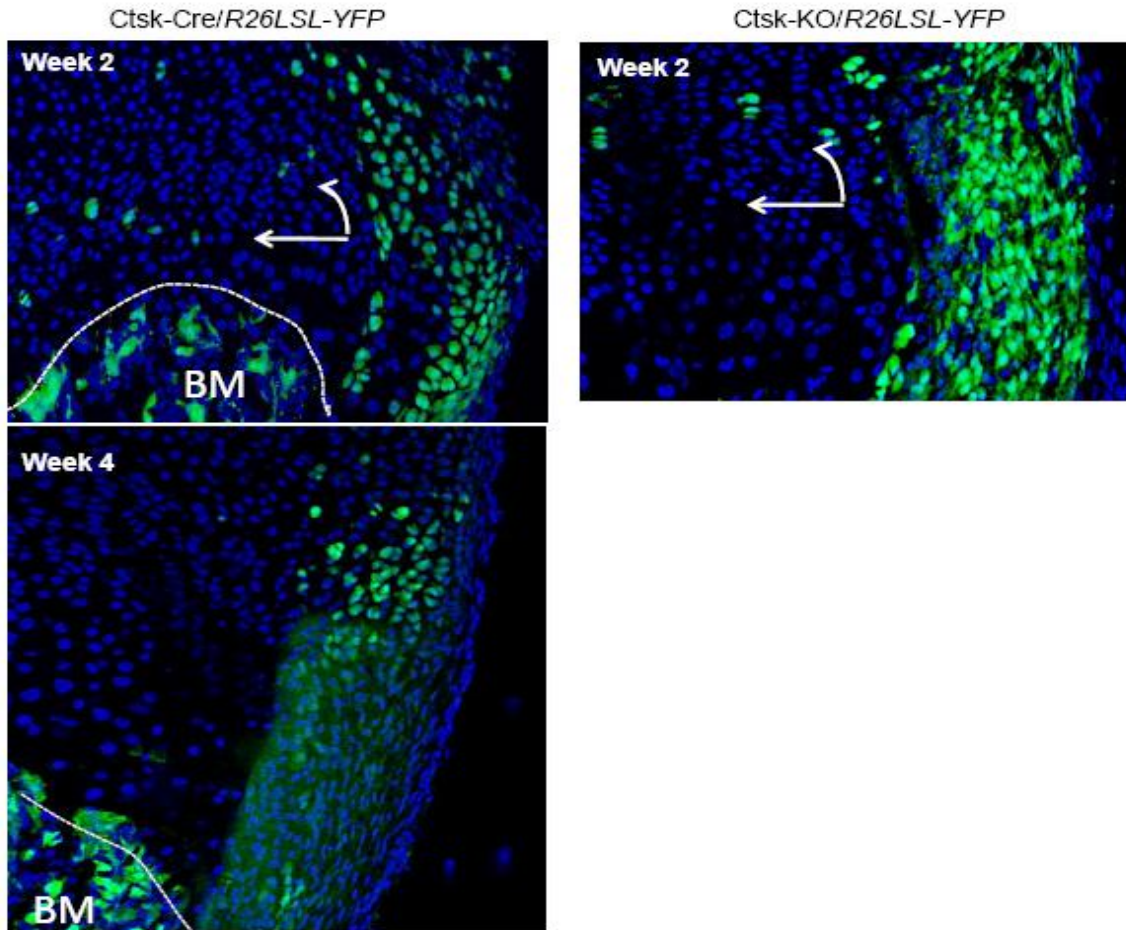


Figure S9 | Confocal fluorescence micrographs showing that the Cathepsin K promoter is active in cells within Perichondrial Groove of Ranvier at post-natal weeks 2 and 4. Note that some of these cells migrate towards the growth plate and articular cartilage (arrows) during normal development. In the absence of *Shp2* (right panel), the number of YFP⁺ cells increases substantially, and they are the primary contributors to the exostoses and enchondromas in *Ctsk*-KO mice. A representative image from one of two mice analyzed for each genotype is shown.

CORRIGENDUM

doi:10.1038/nature13170

Corrigendum: *Ptpn11* deletion in a novel progenitor causes metachondromatosis by inducing hedgehog signalling

Wentian Yang, Jianguo Wang, Douglas C. Moore, Haipei Liang, Mark Dooner, Qian Wu, Richard Terek, Qian Chen, Michael G. Ehrlich, Peter J. Quesenberry & Benjamin G. Neel

Nature **499**, 491–495 (2013); doi:10.1038/nature12396

After publication of this Letter, we became aware that we had not reported the details of construction and validation of our floxed conditional deletion *Ptpn11* allele. These details are presented in the Supplementary Methods and Supplementary Fig. 1 of this Corrigendum. We also stated in our manuscript that *PTPN11* is not mutated in human hepatocellular carcinoma, but it has been brought to our attention that a low frequency of copy number abnormalities involving the *PTPN11* locus in this disorder has been reported¹. However, comparable numbers of amplifications and deletions were observed, making it difficult to conclude from the data in ref. 1 that *PTPN11* acts as a tumour suppressor gene in hepatocellular carcinoma.

Supplementary Information is available in the online version of the Corrigendum.

1. Nalesnik, M. A. *et al.* Gene deletions and amplifications in human hepatocellular carcinomas: correlation with hepatocyte growth regulation. *Am. J. Pathol.* **180**, 1495–1508 (2012).

Supplementary Methods

Generation of a *Ptpn11* conditional deletion allele Clones spanning the *Ptpn11* locus were isolated from a 129/SvJ genomic library. A targeting vector was constructed by inserting lox P sites to flank *Ptpn11* exon11 (**Fig. S1**), followed by a splice acceptor β -galactosidase/pGK-neo cassette (SA β gal pGK/Neo). The diphtheria toxin-A gene also was introduced to facilitate negative selection.

Mouse ESVJ-1182 ES cells (Go Germline; Genome Systems) were cultured on irradiated mouse embryonic fibroblasts (MEFs) in ES cell medium (Dulbecco's modified Eagle's medium containing leukemia inhibitory factor; Gibco BRL, Rockville, MD) at 37°C and 5% CO₂. ES cell propagation, electroporation and selection of recombinants in G418-containing media, and preparation and culture of MEFs and bone marrow-derived macrophages (BMMs) were carried out as described previously^{2,3}. Three correctly targeted ES clones (#49, #79, and #183) were first identified by PCR screening and then confirmed by Southern blots with probe A after digestion with SpeI (b, left). Clones #49 and #79 were later electroporated with the plasmid pGK-Cre. Upon screening, two recombinant clones (J40, I22) carrying the *Ptpn11* floxed allele were identified by PCR and confirmed by Southern blot analysis of EcoRI-digested genomic DNA, using probes B and C (**Fig. S1**).

Chimeras were generated by injecting two of the recombinant ES cell clones into C57BL/6J blastocysts. High percentage chimeras from both clones (which behaved identically) were crossed to C57BL/6J mice to generate heterozygotes. Mice were genotyped for the floxed (430 bp) and wild type *Ptpn11* (312 bp) alleles by PCR (Forward primer F1: 5'-TAG CTG CTT TAA CCC TCT GTG T; Reverse primer R1: 5'-CAT CAG AGC AGG CCA TAT TCC) using tail DNA. PCR conditions for genotyping are available from W.Y. upon request.

Mice carrying one *Ptpn11*-deleted allele ($\Delta K11$) were generated by germ line deletion of the floxed *Ptpn11* allele, following crossing to actin-Cre mice⁴. MEFs bearing one *Ptpn11* $\Delta k11$ allele were derived from E13.5 embryos, as described earlier².

- Yang, W. et al. An Shp2/SFK/Ras/Erk signaling pathway controls trophoblast stem cell survival. *Dev. Cell* 10, 317–327 (2006)
- David, M., Chen, H. E., Goelz, S., Larner, A. C. & Neel, B. G. Differential regulation of the alpha/beta interferon-stimulated Jak/Stat pathway by the SH2 domain-containing tyrosine phosphatase SHPTP1. *Mol Cell Biol* 15, 7050-7058 (1995).
- Lewandoski M; Meyers EN; Martin GR. 1997. Analysis of Fgf8 gene function in vertebrate development. *Cold Spring Harb Symp Quant Biol* 62:159-68.

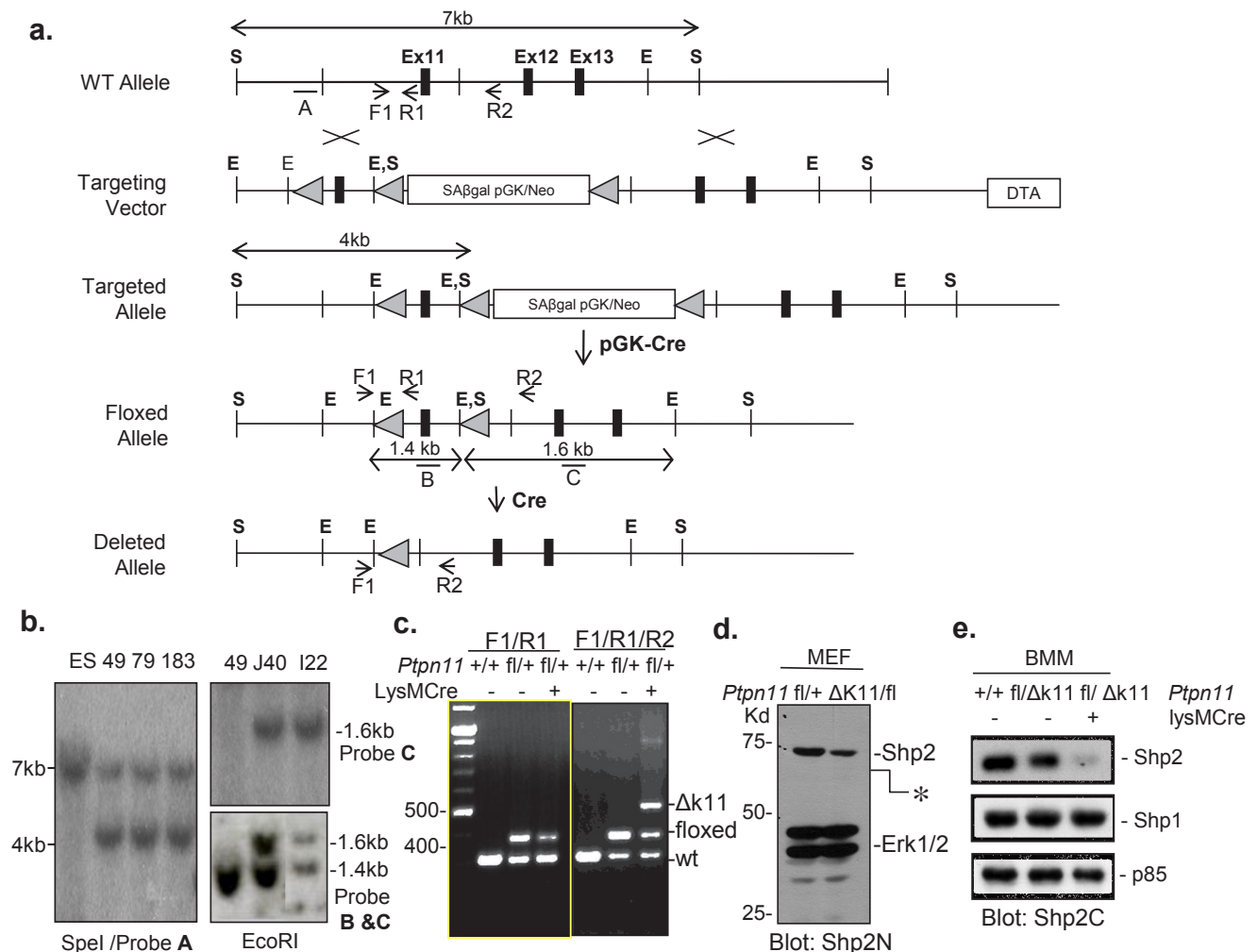


Figure S1 | Generation of inducible (floxed) *Ptpn11* knockout allele. **a**, A targeting vector was constructed to contain LoxP sites flanking *Ptpn11* exon 11, followed by a LoxP-flanked Neo^R cassette. The DT-A (diphtheria toxin-A) gene was included to facilitate negative selection. S: SpeI, E: EcoRI, Ex: exon. F1, R1 and R2 indicate the locations of primers used

to screen for the *Ptpn11* floxed and deleted alleles by PCR. **b**, Southern blots with probes A, C and B+C (as indicated on the diagram) to assess proper generation of the targeted allele (Left panel) and the presence of *Ptpn11* floxed allele (Right panels). Clones #49, #79, and #183 are correctly targeted ES cells bearing the Neo^R cassette; Clones #J40 and #I22 are derivatives of clones #49 and #79, respectively, following successful removal of Neo^R cassette after exposure to pGK-Cre. Note that the germ line (unrearranged) EcoR1 bands expected with probes C and B+C are too big to transfer and be detected in the blot. **c**, PCR analysis with the indicated primer sets showing *Ptpn11* wild type, floxed, and deleted ($\Delta k11$) alleles in genomic DNA extracted from bone marrow derived macrophages (BMM). Note that LysM-Cre-catalyzed deletion is only partial. **d-e**, Immunoblots of total cell lysates (TCL) from the indicated mouse embryonic fibroblasts (MEF) and BMM with anti-Shp2 N-terminal (**d**) and C-terminal antibodies (**e**). Note the efficient deletion of the *Ptpn11* floxed allele in *Ptpn11^{fl}/+* MEF (50% reduction in Shp2 levels) and BMM from LysM-KO (>90% decrease in Shp2) and the absence of any truncated form of Shp2 in mice in which the *Ptpn11^{fl}* allele has been deleted ($\Delta k11$). The asterisk shows the expected size of the Shp2 truncation product that could be generated after Cre-mediated recombination. Note the lack of expression of this (or any other) fragment of Shp2.